Geophys. J. Int. (2004) **159,** 69–82 doi: 10.1111/j.1365-246X.2004.02376.x

An ellipticity criterion in magnetotelluric tensor analysis

M. Becken and H. Burkhardt

Department of Applied Geophysics, Technical University Berlin, Ackerstrasse 71–76, 13355 *Berlin, Germany*

Accepted 2004 May 19. Received 2004 May 19; in original form 2003 May 28

SUMMARY

We examine the magnetotelluric (MT) impedance tensor from the viewpoint of polarization states of the electric and magnetic field. In the presence of a regional 2-D conductivity anomaly, a linearly polarized homogeneous external magnetic field will generally produce secondary electromagnetic fields, which are elliptically polarized. If and only if the primary magnetic field vector oscillates parallel or perpendicular to the 2-D structure, will the horizontal components of the secondary fields at any point of the surface also be linearly polarized. When small-scale inhomogeneities galvanically distort the electric field at the surface, only field rotations and amplifications are observed, while the ellipticity remains unchanged. Thus, the regional strike direction can be identified from vanishing ellipticities of electric and magnetic fields even in presence of distortion. In practice, the MT impedance tensor is analysed rather than the fields themselves. It turns out, that a pair of linearly polarized magnetic and electric fields produces linearly polarized columns of the impedance tensor. As the linearly polarized electric field components generally do not constitute an orthogonal basis, the telluric vectors, i.e. the columns of the impedance tensor, will be non-orthogonal. Their linear polarization, however, is manifested in a common phase for the elements of each column of the tensor and is a well-known indication of galvanic distortion. In order to solve the distortion problem, the telluric vectors are fully parametrized in terms of ellipses and subsequently rotated to the coordinate system in which their ellipticities are minimized. If the minimal ellipticities are close to zero, the existence of a (locally distorted) regional 2-D conductivity anomaly may be assumed. Otherwise, the tensor suggests the presence of a strong 3-D conductivity distribution. In the latter case, a coordinate system is often found, in which three elements have a strong amplitude, while the amplitude of the forth, which is one of the main-diagonal elements, is small. In terms of our ellipse parametrization, this means, that one of the ellipticities of the two telluric vectors approximately vanishes, while the other one may not be neglected as a result of the 3-D response. The reason for this particular characteristic is found in an approximate relation between the polarization state of the telluric vector with vanishing ellipticity and the corresponding horizontal electric field vector in the presence of a shallow conductive structure, across which the perpendicular and tangential components of the electric field obey different boundary conditions.

Key words: 3-D effects, decomposition, galvanic distortion, magnetotelluric impedance tensor, polarization state.

1 INTRODUCTION

In magnetotellurics, the impedance tensor **Z**, linking the horizontal components of electric and magnetic fields **E** and **B** in the frequency domain, reflects the conductivity distribution in some volume below the measurement point. Prior to inverting for a conductivity model, an analysis of the estimated impedance tensor is necessary in order to understand the basic electrical properties of the earth in the area of investigation. A successful analysis prevents misinterpretation of the data with inadequate model assumptions, which underly every type of inversion. The analysis is often trivial in the case of a 1-D and 2-D earth, but when 3-D effects are evident in data, the interpreter must decide whether a 2-D model assumption will be suitable to invert such 3-D data. Such a decision may be based upon the number of degrees of freedom inherent in the impedance tensor, reaching a maximum of eight in the general 3-D case, five in the strict 2-D case and two in the 1-D case.

Magnetotelluric (MT) impedance tensor analysis schemes may be classified into mathematical decompositions and physical decompositions following Groom & Bahr (1992). Among the physical

decompositions, the galvanic distortion model, assuming a (regional) 2-D structure (five degrees of freedom) and a (local) distortion introducing another one or two degrees of freedom, is widely used. Such distortion models are based on the assumption, that the measured electric field is affected by local small-scale inhomogeneities, giving rise to frequency-independent field amplifications (which cannot be resolved) and rotations (one or two additional degrees of freedom, depending upon the geometry of the inhomogeneity) while leaving the magnetic field unchanged (see e.g. Bahr 1988; Groom & Bailey 1989; Smith 1995). Therefore, the distortion model is a quasi-static model, assuming the distorter produces no inductive effects.

Alternatively to the galvanic distortion model, a mathematical decomposition is often used by MT practitioners in order to resolve characteristic properties of a 3-D impedance tensor: LaTorraca et al. (1986), hereafter referred to as LaTo, introduced a modified singular value decomposition (SVD), which is reformulated in terms of the canonical decomposition in Yee & Paulson (1987). These mathematical decompositions are attractive, because the tensor is fully parametrized with eight parameters and no *a priori* assumptions are required. Therefore, in contrast to the distortion analysis, the SVD never fails (at least theoretically). On the other hand, it may be considered a drawback of the method that it is not directly related to any simplifying model, such as a locally distorted regional 2-D structure. In practice, the SVD cannot recover the general distortion model with seven degrees of freedom. This is a consequence of the orthogonality restriction, which is pairwise imposed on the singular vectors, i.e. the principal components of the local electric and magnetic field. In case of six degrees of freedom, however, the SVD yields the same results as the distortion analysis.

We introduce an alternative physical parametrization, which combines the SVD approach and the distortion analysis. In contrast to the SVD, we permit a non-orthogonal basis for the electric polarization states, which is required to adequately account for a general type of galvanic distortion. When such a distortion model fits the data, one or two of the parameters automatically vanish in the regional coordinate system, while the other parameters are directly related to the regional impedances and local distortion parameters. It is shown, that the regional coordinate system is identified from vanishing ellipticities of the columns of the impedance tensor, i.e. the telluric vectors. Based upon our parametrization, an algorithm for simultaneously analysing data at different stations and periods is proposed. Its implementation is very simple and yields stable results. In contrast to standard single site galvanic distortion analyses or the multisite version of McNeice & Jones (2001), we search directly for the regional coordinate system by minimizing the ellipticities of the telluric vectors instead of fitting the distortion model to data. In regional coordinates, the distortion parameters including their error bars are then analytically determined.

If the impedance tensor represents a strong 3-D structure with 3-D inductive effects, our analysis does not fail, however the result may no longer be interpreted in terms of galvanic distortion. In this case, one or both of the telluric vectors are elliptically polarized in any coordinate system. If one of the telluric vectors is found to be linearly polarized at a broad range of periods for one rotation angle, it may physically be connected to a linear polarization state of an electric field. Depending on the position with respect to a shallow conductor, this electric field is then either related to a magnetic source field polarized tangential or perpendicular to the conductor. We observe such cases in our synthetic model studies as well as in our field data.

2 THEORY

We start our analysis by briefly revisiting the galvanic distortion model and its relation to the SVD. The ellipticity parametrization of the impedance tensor, which is the goal of this derivation, is then a straightforward task.

2.1 Galvanic distortion

Following Smith (1995), we assume that the measured local electric field $\mathbf{E}^{\mathrm{l}}$ deviates from a regional electric $\mathbf{E}^{\mathrm{r}}$ field as a result of local galvanic distortion according to the model $\mathbf{E}^{\mathrm{l}} = \mathbf{D}\mathbf{E}^{\mathrm{r}}$, where $\mathbf{D}$ is a real and frequency-independent electric distortion matrix. In absence of distortion, $\mathbf{D}$ is the identity matrix. Bahr's parametrization (Bahr 1988)

$$\mathbf{D} = \begin{bmatrix} g_x \begin{pmatrix} \cos\beta_x \\ \sin\beta_x \end{pmatrix} & g_y \begin{pmatrix} -\sin\beta_y \\ \cos\beta_y \end{pmatrix} \end{bmatrix} \tag{1}$$

has a very intuitive meaning: here, the gain factors g_x and g_y are the (static) shifts, amplifying the regional electric fields in the x and the y directions, respectively. The real quantities β_x and β_y are the clockwise rotation angles of the regional x- and y-field components. The measured (distorted) electric fields give rise to a distorted MT impedance estimate $\mathbf{Z}^{\mathrm{l}}$, which is related to the undistorted regional impedance $\mathbf{Z}^{\mathrm{r}}$ as

$$\mathbf{Z}^{\mathrm{l}} = \mathbf{D}\mathbf{Z}^{\mathrm{r}}. \tag{2}$$

In general, none of the distortion parameters nor the elements of the regional impedance tensor can be deduced from eq. (2) without further assumptions. Therefore, assuming $\mathbf{Z}^{\mathrm{r}}$ represents the response of a regional 2-D structure, eq. (2) reads in regional coordinates as

$$\mathbf{Z}^{\mathrm{l}} = \begin{bmatrix} \cos\beta_x & -\sin\beta_y \\ \sin\beta_x & \cos\beta_y \end{bmatrix} \begin{bmatrix} 0 & g_y Z^{\mathrm{r}}_{xy} \\ g_x Z^{\mathrm{r}}_{yx} & 0 \end{bmatrix}. \tag{3}$$

In measurement coordinates (rotated clockwise with respect to regional coordinates), eq. (3) reads as

$$\mathbf{Z}^{\mathrm{l}'} = \mathbf{R}\mathbf{D}\mathbf{Z}^{\mathrm{r}}\mathbf{R}^{\mathrm{T}}, \tag{4}$$

where $\mathbf{R}$ is a clockwise rotation matrix, the superscript T denotes matrix transpose and the prime denotes the rotated matrix. From eq. (3), it is seen, that in and only in regional coordinates do the elements of each column of $\mathbf{Z}^{\mathrm{l}'}$ have a common phase. This criterion is employed to detect the regional coordinate system, in which the regional impedance tensor and the distortion matrix are uniquely separated aside from the gain factors g_x and g_y.

Distortion analysis has become a standard tool of MT tensor analysis and is applied to determine an appropriate rotation angle for 2-D data analysis and occasionally to separate distortion from the regional signature. Successful examples of galvanic distortion analysis have been reported by many authors, of which a list can be found in McNeice & Jones (2001). Sometimes, however, distortion analysis does not provide a consistent picture. This is the case in the presence of strong 3-D inductive effects.

2.2 Singular value decomposition

The SVD (LaTo) of the 2×2–matrix $\mathbf{Z}$ yields two pairs of normalized complex right- and left-singular vectors $\mathbf{h}_i$ and $\mathbf{e}_i$, respectively, where $i = 1, 2$. Each pair forms an orthonormal basis in the sense

$$\begin{aligned} \mathbf{h}_i^* \cdot \mathbf{h}_j &= \delta_{ij}, \\ \mathbf{e}_i^* \cdot \mathbf{e}_j &= \delta_{ij}, \end{aligned} \tag{5}$$

such that

$$\begin{aligned}\mathbf{Z}\mathbf{h}_i &= r_i\mathbf{e}_i,\\ \widetilde{\mathbf{Z}}\mathbf{e}_i &= r_i\mathbf{h}_i,\end{aligned} \tag{6}$$

where the superscript * denotes complex conjugate, $\widetilde{\mathbf{Z}}$ is the hermitian transpose of $\mathbf{Z}$, $r_1 \geq r_2 \geq 0$ are the real singular values and δ_{ij} is the Kronecker delta. With the ellipse representation of a complex two-component vector described in Appendix A, the singular vectors can be uniquely rewritten in terms of ellipse parameters as

$$\mathbf{v} = e^{i\zeta}\,(a\widehat{\mathbf{a}} + ic\widehat{\mathbf{c}})\,, \tag{7}$$

with real major and minor axes a and c pointing into the directions of the unit vectors $\widehat{\mathbf{a}}$ and $\widehat{\mathbf{c}}$, respectively, where $\widehat{\mathbf{c}} = \widehat{\mathbf{z}} \times \widehat{\mathbf{a}}$, and an initial phase ζ. Note, that our ellipse definition slightly deviates from that of LaTo. As shown in Appendix B, using eq. (7) leads immediately to the complex characteristic values μ_i, the modified singular values suggested by LaTo, which may physically be interpreted in terms of electromagnetic impedances.

The orthogonality (eq. 5) of the singular vectors ($\mathbf{h}_i$, $\mathbf{h}_j$) or ($\mathbf{e}_i$, $\mathbf{e}_j$) is an important constraint on the analysis. It is given in terms of the ellipse parametrization (eq. 7) by

$$e^{i(\zeta_i-\zeta_j)}\,[a_i\widehat{\mathbf{a}}_i - ic_i\widehat{\mathbf{c}}_i]\cdot[a_j\widehat{\mathbf{a}}_j + ic_j\widehat{\mathbf{c}}_j] = \delta_{ij}\,, \tag{8}$$

which states the normalization

$$a_i^2 + c_i^2 = 1 \tag{9}$$

for $i = j$ and the orthogonality

$$\widehat{\mathbf{a}}_i\cdot\widehat{\mathbf{a}}_j = 0, \quad \widehat{\mathbf{c}}_i\cdot\widehat{\mathbf{c}}_j = 0 (i \neq j) \tag{10}$$

of the ellipse axes except for circular polarization. Because $\widehat{\mathbf{a}}_i\cdot\widehat{\mathbf{c}}_i = 0$, it follows from the condition of eq. (10), that $\widehat{\mathbf{a}}_i\cdot\widehat{\mathbf{c}}_j = \pm 1$, which can only be true from eq. (8) if the ellipticities $|\epsilon_i| = |c_i/a_i|$ are the same for i and j. Thus, non-orthogonal linear polarization states of some principal electric and/or magnetic field vectors are represented in orthogonal but elliptical polarization states. Therefore, the SVD of LaTo is not suitable to describe the situation of galvanic distortion of regional 2-D fields as defined in the expressions of eqs (3) and (4), where the distorted electric field components constitute an non-orthogonal basis.

The modified SVD parametrization of the impedance tensor reads in matrix notation as

$$\mathbf{Z} = \mathbf{U}_e\mathbf{M}\widetilde{\mathbf{U}}_h, \tag{11}$$

where the columns of the unitary matrices $\mathbf{U}_e$ and $\mathbf{U}_h$ are phase modified singular vectors $\boldsymbol{e}_i e^{-i\zeta_{e,i}}$ and $\boldsymbol{h}_i e^{-i\zeta_{h,i}}$, respectively, and $\mathbf{M} = \mathrm{diag}(\mu_1, \mu_2)$.

Theses characteristic impedances μ_i as well as the direction of singular vectors are supposed to give a better insight into the 3-D conductivity distribution than the impedance tensor itself (LaTo). However, the method was not designed with the background of a particular physical model as for instance the distortion model in eq. (2) is. It is therefore not surprising that the modified SVD of a galvanically distorted 2-D impedance of the form of eq. (3) generally does not yield the regional impedances nor the distortion parameters, nor the regional strike direction, as reported for instance in Groom & Bailey (1991). The reason is given in terms of the orthogonality imposed on the singular vectors, while the distorted horizontal components of the regional electric field are at most incidentally orthogonal in the regional coordinate system. There are however some indications deducible from the outcome of the SVD, which point towards the existence of a (distorted) regional 2-D structure. They have partly been reported in Groom & Bailey (1991) and are summarized and proven in Appendix C.

In the following section, we will introduce an alternative approach, which is related to the modified SVD, because it relies on principal vectors, but their orthogonality is removed. By doing so, the general case of galvanic distortion is also covered.

2.3 The ellipticity of telluric vectors

Let us assume for simplicity that according to eq. (7) the local horizontal magnetic field

$$\mathbf{B} = e^{i\zeta_B}a_B\widehat{\mathbf{a}}_B \tag{12}$$

is linearly polarized with phase ζ_B, amplitude a_B and direction $\widehat{\mathbf{a}}_B$. The horizontal electric field $\mathbf{E} = \mathbf{Z}\mathbf{B}$ is in general elliptically polarized and represented in the form

$$\mathbf{E} = e^{i\zeta_E}\,(a_E\widehat{\mathbf{a}}_E + ic_E\widehat{\mathbf{c}}_E)\,. \tag{13}$$

Further assume a coordinate system, in which the magnetic field $\mathbf{B}_1$ is given with direction $\widehat{\mathbf{a}}_{B,1} = (1, 0)^T$ and the corresponding electric field $\mathbf{E}_1 = \mathbf{Z}\mathbf{B}_1$ with $\widehat{\mathbf{a}}_{E,1} = (\cos\alpha_{E,1}, \sin\alpha_{E,1})^T$ and $\widehat{\mathbf{c}}_{E,1} = (-\sin\alpha_{E,1}, \cos\alpha_{E,1})^T$. Combining eqs (12) and (13) with the impedance relation yields, after rearrangement for the column vector $\mathbf{e}_x = (Z_{xx}, Z_{yx})^T$,

$$\mathbf{e}_x = e^{i\zeta_x}\,(a_x\widehat{\mathbf{a}}_{E,1} + ic_x\widehat{\mathbf{c}}_{E,1})\,, \tag{14}$$

where $a_x = a_{E,1}/a_{B,1}$, $c_x = c_{E,1}/a_{B,1}$, $\zeta_x = \zeta_{E,1} - \zeta_{B,1}$. The same parametrization applies to $\mathbf{e}_y = (Z_{xy}, Z_{yy})^T$ for the magnetic field $\mathbf{B}_2$ with direction $\widehat{\mathbf{a}}_{B,2} = (0, 1)^T$ and the electric field $\mathbf{E}_2$ with $\widehat{\mathbf{a}}_{E,2} = (\cos\alpha_{E,2}, \sin\alpha_{E,2})^T$ and $\widehat{\mathbf{c}}_{E,2} = (-\sin\alpha_{E,2}, \cos\alpha_{E,2})^T$ yielding

$$\mathbf{e}_y = e^{i\zeta_y}(a_y\widehat{\mathbf{a}}_{E,2} + ic_y\widehat{\mathbf{c}}_{E,2}), \tag{15}$$

where $a_y = a_{E,2}/a_{B,2}$, $c_y = c_{E,2}/a_{B,2}$, $\zeta_y = \zeta_{E,2} - \zeta_{B,2}$. Following Bahr (1988), the columns of $\mathbf{Z}$ are referred to as telluric vectors. They obey the same polarization state as the input electric fields $\mathbf{E}_1$ and $\mathbf{E}_2$, i.e. they are orientated in the same direction and have the same ellipticity. Thus, the ellipse representation of electric and magnetic fields yields a parametrization of the impedance tensor in terms of elliptically polarized telluric vectors $\mathbf{e}_i$. Observe, that the normalized versions of $\mathbf{B}_1$ and $\mathbf{B}_2$ satisfy the orthogonality criterion (eq. 5), while $\mathbf{E}_1$ and $\mathbf{E}_2$ are not orthogonal. Expanding the expressions of eqs (14) and (15) for $\mathbf{Z}$ and substituting for notational simplicity $\alpha_x = \alpha_{E,1}$ and $\alpha_y = \alpha_{E,2}$ yields

$$\begin{aligned}\mathbf{Z} = &\begin{bmatrix}\cos\alpha_y & \cos\alpha_x\\ \sin\alpha_y & \sin\alpha_x\end{bmatrix}\begin{bmatrix}0 & a_y e^{i\zeta_y}\\ a_x e^{i\zeta_x} & 0\end{bmatrix} +\\ &\begin{bmatrix}-i\sin\alpha_y & -i\sin\alpha_x\\ i\cos\alpha_y & i\cos\alpha_x\end{bmatrix}\begin{bmatrix}0 & c_y e^{i\zeta_y}\\ c_x e^{i\zeta_x} & 0\end{bmatrix}.\end{aligned} \tag{16}$$

Introducing the ellipticity $\epsilon_i = c_i/a_i$, eq. (16) maybe rewritten as

$$\mathbf{Z} = \mathbf{C}\mathbf{Z}^{\mathrm{r}}, \tag{17}$$

where

$$\mathbf{C} = \begin{bmatrix}\cos\alpha_y & \cos\alpha_x\\ \sin\alpha_y & \sin\alpha_x\end{bmatrix} + i\begin{bmatrix}-\epsilon_y\sin\alpha_y & -\epsilon_x\sin\alpha_x\\ \epsilon_y\cos\alpha_y & \epsilon_x\cos\alpha_x\end{bmatrix}$$

and

$$\mathbf{Z}^{\mathrm{r}} = \begin{bmatrix}0 & a_y e^{i\zeta_y}\\ a_x e^{i\zeta_x} & 0\end{bmatrix}.$$

Thus, the impedance tensor $\mathbf{Z}$ can be represented by an antidiagonal characteristic impedance tensor $\mathbf{Z}^{\mathrm{r}}$ and a complex-valued matrix $\mathbf{C}$, describing the polarization characteristics.

The decomposition (eq. 17) of the impedance tensor is a full parametrization requiring eight degrees of freedom. Using elliptically polarized magnetic and electric fields at the same time yields indistinguishable parametrizations but with the loss of their simple interpretability in terms of field polarization ellipses. The parameters in the expression of eq. (17) will rather be an algebraic mixture of the fields of both polarizations, as will be shown in Section 2.3.2.

2.3.1 Galvanic distortion model

Because the parametrization of eq. (17) covers all possible degrees of freedom in the given coordinate system, any rotation into another coordinate system, where the rotation angle is an additional parameter, introduces a dependency. Thus, two rotation angles δ_x and δ_y must exist, where one of the ellipticities ϵ_x and ϵ_y vanishes. If, in addition, $\delta_{\mathrm{x}} = \delta_{\mathrm{y}}$, the number of degrees of freedom of the tensor drops to seven. In this case, the second addend of $\mathbf{C}$ in eq. (17) vanishes and $\mathbf{C}$ becomes real. This states, with the review of eqs (14) and (15), that the telluric vectors are linearly polarized while no restrictions are imposed on α_x and α_y, i.e. the directions of the (now linearly) polarized electric field.

Physically, vanishing ellipticities of both telluric vectors in the same coordinate system may be interpreted in terms of linear polarization states of pairs of electric and magnetic fields, as can be deduced from eq. (16) with $c_{x,y} = 0$. Such polarization states, if occurring independent of period, may only be observed in the presence of a 1-D earth or a 2-D conductivity distribution, where in the latter case the fields must be oscillating in the principal directions of the 2-D structure. Otherwise, or in the presence of a (strong) 3-D distribution, the electromagnetic fields will generally be elliptically polarized. Galvanic distortion of the electric fields as a result of small inhomogeneities does not change their polarization states, but may alter their directions of oscillation. Therefore, $\alpha_{x,y}$ do only coincide with the coordinate axes in the absence of galvanic distortion.

By comparison of the parametrizations of eqs (3) and (17) with $\epsilon_i = 0$,

$$g_x Z^{\mathrm{r}}_{yx} = a_x e^{i\zeta_x}, \quad g_y Z^{\mathrm{r}}_{xy} = a_y e^{i\zeta_y} \tag{18}$$

are identified as the regional impedances and

$$\alpha_x = \beta_y + \frac{\pi}{2}, \quad \alpha_y = \beta_x \tag{19}$$

are related to the distortion angles.

Therefore, we conclude, that if a coordinate system exists, in which the ellipticities of the telluric vectors $\mathbf{e}_x$ and $\mathbf{e}_y$ vanish, i.e. $\epsilon_x = \epsilon_y = 0$ for $\delta_x = \delta_y$, then the galvanic distortion model is satisfied, the underlying magnetic states are linear and orthogonal, and the electric states are linear but not necessarily orthogonal. This opens a strategy for seeking the regional coordinate system, which is formulated in Section 2.4 in terms of an optimization problem.

If no such coordinate system exists, the tensor represents a strong 3-D structure with eight degrees of freedom. Though the impedances in the representation of eq. (17) can be considered as some type of characteristic impedances following LaTo, we can not connect them to a physical model simpler than a 3-D model. Occasionally, the ellipse parameters might give better insight into the nature of the 3-D problem than the pure impedance elements (apparent resistivities and phase) do. Such a case is discussed in Section 2.3.2 and illustrated in Section 3.2.2.

2.3.2 3-D effects

As we mentioned in the previous section, there always exists one rotation angle for each period, for which one of the ellipticities ϵ_x or ϵ_y must vanish. This rotation angle has not necessarily a physical relevance in terms of the polarization states of the horizontal electromagnetic field components, because it may be determined for any combination of elliptically polarized electric and magnetic fields.

However, as a result of different boundary conditions for the perpendicular and tangential components of the electric field at lateral contrasts, the polarization state of one of the telluric vectors will often be dominated by the corresponding horizontal electric field. This can be shown as follows. Assume two orthogonal normal magnetic fields $\mathbf{B}_{1,n} = B_n\widehat{\mathbf{x}}$ and $\mathbf{B}_{2,n} = B_n\widehat{\mathbf{y}}$, oscillating collinear with the coordinate axes. The total magnetic fields are then given by $\mathbf{B}_{1,2} = \mathbf{B}_{1,2,n} + \mathbf{B}_{1,2,a}$, where $\mathbf{B}_a$ denotes the anomalous fields, and are connected to the electric fields via the local impedance $\mathbf{Z}$ as $\mathbf{E}_{1,2} = \mathbf{Z}\mathbf{B}_{1,2}$. Following for example Zonge & Hughes (1991), the first column of the impedance tensor, i.e. the telluric vector $\mathbf{e}_x$, is given by

$$\mathbf{e}_x = \mathbf{E}_1 c B_{y,2} - \mathbf{E}_2 c B_{y,1}, \tag{20}$$

where $c = B_{x1}B_{y2} - B_{x2}B_{y1}$ may be regarded as a complex constant. Each of the electric field vectors may be rewritten in terms of the ellipse parametrization of eq. (13) yielding

$$\mathbf{e}_x = c a_{E,1} B_{y,2} \widetilde{\mathbf{e}}_{E,1} - c a_{e,2} B_{y,1} \widetilde{\mathbf{e}}_{E,2}, \tag{21}$$

where $\widetilde{\mathbf{e}}_{E,1,2}$ are the electric field ellipses normalized by their major axes $a_{E,1,2}$, i.e. by the amplitude of the electric field vector. A similar parametrization applies to $\mathbf{e}_y$:

$$\mathbf{e}_y = -c a_{E,1} B_{x,2} \widetilde{\mathbf{e}}_{E,1} + c a_{e,2} B_{x,1} \widetilde{\mathbf{e}}_{E,2}. \tag{22}$$

Thus, the telluric vector $\mathbf{e}_x(\mathbf{e}_y)$ is generally the superposition of the normalized electric fields scaled by their amplitudes a_E and the amplitude of the magnetic field components in y direction (x direction). In the 2-D case (including galvanic distortion), eqs (21) and (22) reduce to eqs (14) and (15) with $c_{x,y} = 0$, respectively, because $B_{y,1}$ and $B_{x,2}$ vanish identically in a coordinate system aligned with the strike direction.

Let us now consider a 3-D conductivity distribution with a conductive surface anomaly and let the x-axis be tangential to the shallow conductivity contrast. Then, the fields $\mathbf{B}_1$, $\mathbf{E}_1$ may be considered as local B-polarization (i.e. the normal part of $\mathbf{E}_1$ is orientated normal to the contrast), while $\mathbf{B}_2$, $\mathbf{E}_2$ are in local E-polarization (normal part of $\mathbf{E}_2$ tangential to the contrast). In the vicinity of the lateral contrast, but on the resistive side, the electric field in local B-polarization (more precisely, the component normal to the contrast) is amplified as a result of the galvanic-like charge accumulation at the discontinuity, while the electric field in local E-polarization is attenuated. Hence, $a_{E,1} > a_{E,2}$. Moreover, $|B_{y,2}| = |B_n + B_{a,y,2}| > |B_{y,1}| = |B_{a,y,1}|$, because the anomalous magnetic field is usually smaller than the normal magnetic field. Combining the two inequalities yields for many cases a domination of the corresponding telluric vector by the local B-polarization electric field on the resistive side of the conductivity contrast (even in the presence of 3-D effects) as a result of $|a_{E,1}B_{y,2}| \gg |a_{E,2}B_{y,1}|$, i.e.

$$\mathbf{e}_x \simeq c a_{E,1} B_{y,2} \widetilde{\mathbf{e}}_{E,1}. \tag{23}$$

On the other hand, $|B_{x,1}| = |B_n + B_{a,x,1}| > |B_{x,2}| = |B_{a,x,2}|$, which means that in review of eq. (22) the contribution of the strong local B-polarization electric field $\mathbf{E}_1$ to the telluric vector $\mathbf{e}_y$ is scaled down (but may not be neglected in the 3-D case), while the weaker

local E-polarization electric field $\mathbf{E}_2$ becomes more important. Thus, an approximate interpretation of $\mathbf{e}_y$ in terms of the polarization of the electric field is, in this coordinate system, not possible. It will rather reflect the 3-D response.

On the conductive side of the contrast, the situation is different. Here, the local B-polarization electric field is strongly attenuated as a result of the charge accumulation. Thus, $a_{E,1} < a_{E,2}$, which gives in conjunction with the inequalities for the magnetic field that

$$\mathbf{e}_y \simeq -ca_{E,2}B_{x,1}\tilde{\mathbf{e}}_{E,2}. \tag{24}$$

For $\mathbf{e}_x$ no simplifying approximation applies.

Therefore, we conclude, that in the given coordinate system, one of the telluric vectors ($\mathbf{e}_x$ on the resistive side and $\mathbf{e}_y$ on the conductive side) basically represents the polarization state of one electric field vector ($\mathbf{E}_1$ and $\mathbf{E}_2$, respectively).

Assume now further, that for some reason these electric fields are predominantly linearly polarized and aligned with the coordinate axes, i.e. that $\mathbf{E}_1 \simeq E_n\widehat{\mathbf{y}} + E_{y,1,a}\widehat{\mathbf{y}}$ on the resistive side and $\mathbf{E}_2 \simeq E_n\widehat{\mathbf{x}} + E_{x,2,a}\widehat{\mathbf{y}}$ on the conductive side, which is in agreement with the previous approximations. This has the consequence that, on the resistive side of the shallow anomaly, the amplitude of Z_{xx} is small and those of Z_{xy}, Z_{yx} and Z_{yy} can be strong, while on the conductive side, the amplitude of Z_{yy} is small and those of Z_{xx}, Z_{xy} and Z_{yx} can be strong. Thus, an explanation could be given for the observation that in a particular coordinate system, i.e. the local coordinate system, the tensor is often composed of three large elements and one small element. If, additionally, galvanic distortion is present, all four elements might be large, but the ellipticity of the linearly polarized telluric vector remains unchanged, i.e. linear, as can be easily seen from eq. (2) with either $Z^{\mathrm{r}}_{xx} = 0$ or $Z^{\mathrm{r}}_{yy} = 0$.

The validity of the approximations given here may not be generalized, but depends on the particular conductivity model. However, in the later discussed synthetic example 2, we recover the above described properties of the impedance tensor and we are also aware of many field data showing such a behaviour.

2.4 Minimization of ellipticities by rotation

We have shown in Section 2.3.1 that a solution to the galvanic distortion problem can be obtained in terms of vanishing ellipticities of the telluric vectors. For a numerical treatment, the optimization problem is formulated as follows. Find the coordinate system δ, in which the ellipticities of the telluric vectors are minimal. Thus,

$$F(\mathbf{R}(\delta)\mathbf{Z}\mathbf{R}(\delta)^{-1}) = \min!, \tag{25}$$

where $F(\delta)$ is a function yielding the sum of squared ellipticities $\epsilon_i^2(\mathbf{e}_i)$ in the rotated coordinate system, e.g.

$$F(\delta) = \sum_{i=1}^{2} \epsilon_i^2(\mathbf{e}_i). \tag{26}$$

The ellipticities are analytically calculated with formulae in eq. (A7) (Appendix A) from rotated impedances. In the case of real data, the derived ellipticities contain errors and a weighting is required when simultaneously considering both vectors. Letting σ_{ϵ_i} be the standard deviation of $\epsilon_i(\mathbf{e}_i)$, the optimization problem is weighted according to

$$F(\delta) = \sum_{i=1}^{2} \left(\epsilon_i^2(\mathbf{e}_i)/\sigma_{\epsilon_i}^2\right). \tag{27}$$

In order to stabilize the problem, one might want to include several periods $p = 1, \ldots, P$ and sites $k = 1, \ldots, K$ as suggested by McNeice & Jones (2001). This is easily accomplished by expanding the expression of eq. (27) to

$$F(\delta) = \sum_{k=1}^{K}\sum_{p=1}^{P}\sum_{i=1}^{2} \left(\epsilon_{i,k,p}^2(\mathbf{e}_{i,k,p})/\sigma_{\epsilon_{i,k,p}}^2\right). \tag{28}$$

As $F(\delta)$ is a scalar function dependent on only one variable, minimization is quite simple. Here we use a combination of golden section search and parabolic interpolation, an algorithm, found in many mathematical computer packages (e.g. MATLAB). Alternatively, following Zhang *et al.* (1987) one can rotate stepwise through the interval $0 < \delta \leq \pi/2$, determining the strike angle as the angle that yields a minimum $F(\delta)$.

Having found an appropriate rotation angle δ, all parameters (a_x, a_y, c_x, c_y, ζ_x, ζ_y, α_x, α_y) for each site and period may be derived analytically from the rotated impedance tensor $\mathbf{Z}^{\mathrm{l}}$. Moreover, the associated error bars are calculated by linear error propagation using the equations of Appendix A. For ideal regional 2-D data, all $c_i = 0$, but in practice this will not hold true when a broad period band and site range are simultaneously minimized.

The local strike direction, introduced in Section 2.3.2, may be determined by minimizing the ellipticity of only one telluric vector, say $\mathbf{e}_y$ for a number of periods simultaneously. It does not make sense to permit for a multiple site analysis, because the local strike may change form site to site. Therefore, we define the solution δ_y of

$$F(\delta) = \sum_{p=1}^{P} \left(\epsilon_{y,p}^2/\sigma_{\epsilon_{y,p}}^2\right) = \min!, \tag{29}$$

as the local strike. Note, that in contrast to the regional strike direction, δ_y has an ambiguity of 180°.

3 SYNTHETIC EXAMPLES

3.1 Example 1: galvanic distortion analysis

To illustrate the performance of the optimization routine proposed above, we consider a synthetic data example with defined statistical parameters. Here, we take a 2-D regional apparent resistivity tensor with strike direction $\delta = 0°$ and off-diagonal apparent resistivities and phases $\rho_{xy} = 300\ \Omega$m, $\rho_{yx} = 150\ \Omega$ m, $\phi_{xy} = 30°$ and $\phi_{xy} = 41°$, respectively. From these data, 31 regional impedance tensors have been constructed for the period range from 0.001–100 s. Galvanic distortion of the impedances is generated using eq. (3) with $g_x = g_y = 1$, $\beta_x = 23°$ and $\beta_y = -27°$. To produce noisy realizations, gaussian noise with a standard deviation of 5 per cent of the largest impedance magnitude and modified with a random phase between 0° and 360° was added to the distorted tensor at each period. These data, shown in Fig. 1(a), are comparable to those from the first example of McNeice & Jones (2001), because the ratio of apparent resistivities, the phases, distortion parameters and noise level are similar. However, in contrast to McNeice & Jones (2001), we take into account the period dependence inherent in the impedances, which should cancel out in the ellipticties of the telluric vectors.

Minimizing eq. (28) yields a regional strike direction $\delta^o = -0.3°$, which is close to the true strike. Here, the superscript o denotes the optimal estimates. In this coordinate system, ellipticities and distortion angles have been calculated with the formulae in eqs (A8) and (A10) and their associated standard deviations from the variances given in Appendix A3 and A4. They are depicted in Fig. 1. Open circles and triangles correspond to parameters derived from the first ($\mathbf{e}_x$) and second column ($\mathbf{e}_y$) of the tensor, respectively. Dash-dotted

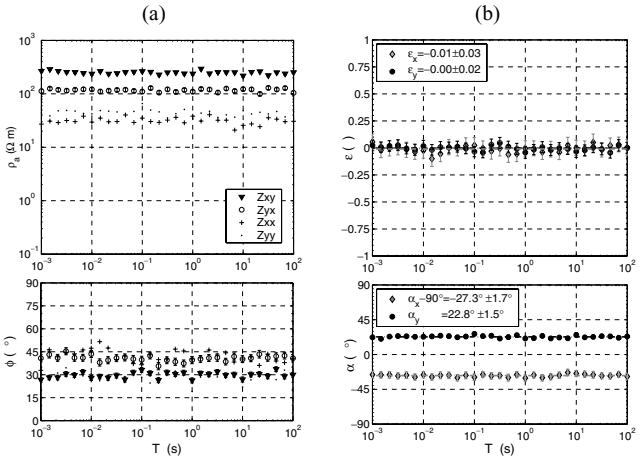

Figure 1. Example 1. (a) Thirty-one noisy and distorted realizations of apparent resistivities and phases for testing the performance of the minimization routine. The distortion matrix is constructed with distortion angles $\beta_x = 23^\circ$ and $\beta_y = -27^\circ$ and unity gain factors. (b) Ellipticities ϵ_x and ϵ_x and related directions of major axes α_x and α_y determined from joint optimization of 31 periods. Symbols indicate individual estimates in the regional coordinate system, dash-dotted lines denote their weighted means.

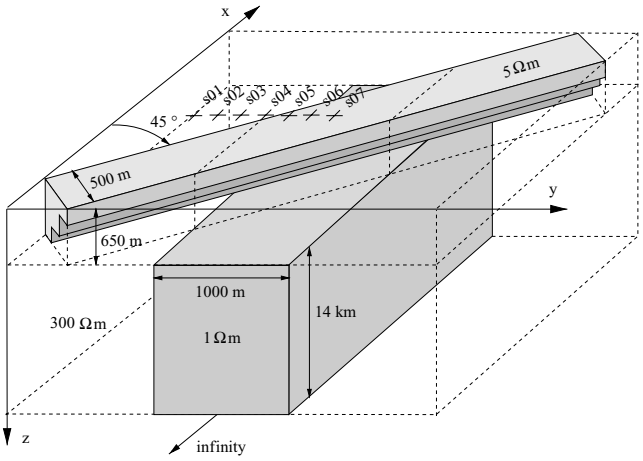

Figure 2. Example 2: sketch of the 3-D model. Two elongated and electrically coupled conductors with a relative orientation of 45° are embedded in a resistive half-space. The model attempts to represent a combination of 2-D, strong 3-D and regional 2-D structure with local distortion for small, medium and large skin depths, respectively. It serves to illustrate the ellipticity analysis, which has been applied to synthetic impedance tensors, generated with a 3-D modelling programme. A profile with seven stations s01–s07 is indicated, for which a set of noise contaminated impedance tensors has been created. They were subjected to the multisite multiperiod optimization routine in order to determine the geoelectric strike direction.

lines in Fig. 1 indicate the weighted means of the related parameter distributions. A quality criterion of the optimization is given in terms of weighted mean ellipticities and the standard deviation of the individual estimates from their mean.

For this example, $\overline{\epsilon}^o_x(\mathbf{e}_x) = -0.01 \pm 0.03$ and $\overline{\epsilon}^o_y(\mathbf{e}_y) = 0.00 \pm 0.02$, indicating a correct determination of the regional coordinate system. Distortion angles are constant with respect to frequency and recovered with mean values $\overline{\alpha}^o_x - 90^\circ = -27.3 \pm 1.7^\circ$ and $\overline{\alpha}^o_y = 22.8 \pm 1.5^\circ$, close to the true values of β_y and β_x. Major axes a^o_x and a^o_y of the telluric vectors are related to the regional apparent resistivities ρ^o_{yx} and ρ^o_{xy}, and their phases ϕ^o_{yx} and ϕ^o_{xy} are given by the initial phases ζ^o_x and ζ^o_y, respectively. Their mean values are recovered to $\overline{\rho}^o_{xy} = 300.1 \pm 13.6\,\Omega$m, $\overline{\rho}^o_{yx} = 152.9 \pm 9.3\,\Omega$m and $\overline{\phi}^o_{xy} = 29.9 \pm 1.2^\circ$, $\overline{\phi}^o_{yx} = 42.0 \pm 1.8^\circ$, which is again close to the true values. Note, that the standard deviation of the individual estimates is of the order of the noise level added to the data previously. This verifies that the propagation of errors does not introduce severe bias in error levels.

Alternatively, the regional impedances may be obtained from inversion of eq. (3), if the distortion parameters are determined. Here, we used the mean of the distortion angles $\overline{\alpha}^o_x - 90^\circ$ and $\overline{\alpha}^o_y$ in order to construct the inverse of the distortion matrix $\mathbf{D}^{-1}$ and derived an estimate of the regional impedance in rotated coordinates with $\mathbf{Z}^{\mathrm{r}} = \mathbf{D}^{-1}\,\mathbf{Z}$. This leads to regional apparent resistivities and phases $\overline{\rho}^o_{xy} = 292.2 \pm 18.5\,\Omega$m, $\overline{\rho}^o_{yx} = 154.7 \pm 15.6\,\Omega$m, $\overline{\phi}^o_{xy} = 30.3 \pm 1.9^\circ$ and $\overline{\phi}^o_{yx} = 41.6 \pm 2.9^\circ$, respectively. These results are slightly less accurate than those obtained from the ellipse parameters. We do not generalize this, because the generation of synthetic noise and error bars might not meet real conditions exactly. Furthermore, real data are never exactly 2-D such that the main-diagonal elements of the impedance tensor vanish exactly as assumed when interpreting the ellipse major axes as regional impedance magnitudes. Nevertheless, this somewhat unrealistic example demonstrates that our algorithm produces statistically reasonable and reproducible results with an accuracy similar to that reported in McNeice & Jones (2001).

3.2 Example 2: a 3-D model

A 3-D modelling programme (Mackie *et al.* 1994) has been used to generate a realistic synthetic data set. Here, we use a model with a comparatively large surface inhomogeneity deviating from a typical galvanic distortion model. It has been designed not only to produce distorted 2-D fields, but also to generate strong 3-D effects within the modelled period range, because we want to demonstrate both the distortion analysis and the parametrization of a 3-D impedance.

The model, sketched in Fig. 2, combines two elongated conductive anomalies embedded in a 300-Ωm half-space. The upper conductor represents the 5-Ω m sedimentary filling of a medium-scale, NE-striking half graben. Being 500-m wide, it extends to the depth of 650 m at its left boundary. The lower conductor is electrically coupled with the graben sediments. It extends between the depth interval from 650 m to 14 km, is 1-km wide and extends to infinity in N/S directions. Its strike direction is 45° counter-clockwise with respect to the surface conductor. Such a structure may, for example, be attributed to a fault zone with fluid-filled fractures giving rise to the conductivity of 1 Ωm.

The model core has been discretized with 70 × 70 × 30 cells in the *x*, *y* and *z* direction, respectively. The smallest cell size is 50 × 50 × 25 m, progressively being increased to depth and, when sufficiently far away from the boundaries of the surface conductor, in horizontal directions. For this model, the MT impedance tensor has been calculated for periods between 0.001–100 s.

The data at seven locations s01–s07 along a profile perpendicular to the regional (lower) conductor and with a site separation of 100 m (Fig. 2) are first considered in this model study. They have been contaminated with 5 per cent gaussian noise, as in the previous example. All sites exhibit 3-D effects between 0.1–100 s. Upon inspection, the data can be classified into three subsets: the short-period part (∼0.001–0.005 s for stations s01–s04, located outside of the surface conductor, and ∼0.001–0.025 s for stations s05–s07, placed on the top of the surface anomaly) is predominantly

sensitive to the shallow conductor. Between ∼0.01–1 s, depending on the station, data are strongly 3-D, because the fields are sensitive to both the shallow and the deep conductor. For periods longer than a few seconds, the skin depth exceeds several kilometres and currents are predominantly induced in the deeper, regional structure. However, the surface conductor continues to act on the regional electric fields as a galvanic distorter even when the anomalous magnetic fields induced within become negligible. Thus, 3-D effects should be explained with a distortion model.

3.2.1 Strike detection and galvanic distortion analysis

The period subsets defined above span a range of periods, because their sensitivities to the conductors vary between stations depending on the distance to them. For the short-period part, we have grouped and simultaneously analysed stations s01–s04 and s05–s07 in the period ranges given above, respectively. In the long-period section, all stations have been grouped together for the purpose of a multisite and multiperiod regional strike detection. All sites in each group are treated equally for simplicity. The period range, for which the retrieved strike direction is actually valid, may be determined later by inspecting the ellipticities at each site individually.

In Table 1, the results of a joint analysis are listed for all sites. Within the short-period band, the first group recovers a strike direction of $\delta^o = 46.3^\circ$, while the second group yields $\delta^o = 46.9^\circ$: both close to the true direction of $\delta = 45.0^\circ$. In both groups, mean ellipticities (here, root mean square of $\overline{\epsilon}^o_x$ and $\overline{\epsilon}^o_y$) and distortion angles $\overline{\beta}^o_x$ and $\overline{\beta}^o_y$ nearly vanish, as can be seen in Table 1(a) and (b). Thus, the 2-D surface structure is clearly expressed in the ellipse parameters.

Table 1. Example 2: ellipse parameters from joint minimization.

Site	$\overline{\epsilon}^o = \sqrt{\overline{\epsilon}^{o2}_x + \overline{\epsilon}^{o2}_y}$	$\overline{\alpha}^o_x - 90^\circ = \overline{\beta}^o_y$	$\overline{\alpha}^o_y = \overline{\beta}^o_x$
(a)	0.001–0.006 s	$\delta^o = 46.3^\circ$	s01–s04
s01	0.01 ± 0.04	0.9 ± 0.6	0.2 ± 2.4
s02	0.03 ± 0.04	0.0 ± 0.9	0.5 ± 2.5
s03	0.01 ± 0.04	0.6 ± 1.4	1.3 ± 2.0
s04	0.05 ± 0.05	1.3 ± 0.8	0.6 ± 3.7
(b)	0.001–0.025 s	$\delta^o = 46.9^\circ$	s05–s07
s05	0.01 ± 0.04	0.8 ± 3.3	-1.2 ± 0.7
s06	0.01 ± 0.05	-0.8 ± 2.0	0.4 ± 0.9
s07	0.02 ± 0.06	-0.2 ± 1.8	-0.4 ± 1.7
(c)	4–100 s	$\delta^o = -0.6^\circ$	s01–s07
s01	0.00 ± 0.04	10.5 ± 1.2	-18.5 ± 2.2
s02	0.01 ± 0.03	16.1 ± 1.4	-20.1 ± 1.9
s03	0.02 ± 0.03	23.5 ± 1.1	-19.6 ± 1.2
s04	0.03 ± 0.04	23.7 ± 1.5	-10.1 ± 2.4
s05	0.02 ± 0.02	-37.7 ± 1.2	41.6 ± 1.2
s06	0.03 ± 0.03	-35.3 ± 1.3	41.0 ± 1.5
s07	0.03 ± 0.04	-35.4 ± 1.6	41.0 ± 1.4

Notes:
Root mean square ellipticities $\overline{\epsilon}^o$ and mean distortion angles $\overline{\beta}^o_x$, $\overline{\beta}^o_y$ in the optimal coordinate system δ^o estimated by multisite multiperiod analysis.
(a) Results for group s01–s04 and periods 0.001–0.006 s.
(b) Results for group s05–s07 and periods 0.001–0.025 s.
(c) Results for group s01–s07 and periods 1–100 s.
The given standard deviation of the parameters from their weighted mean indicates the consistency of the parameters with respect to the frequency band.

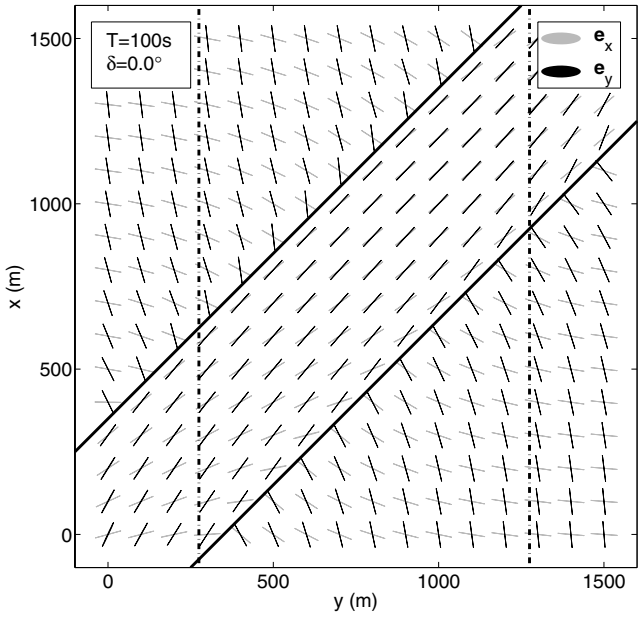

Figure 3. Example 2: ellipses (normalized by the length of their major axes), calculated for the period $T = 100$ s in the regional coordinate system (0°), representing the polarization state of telluric vectors. Dash-dotted and solid lines indicate strike direction and boundaries of the regional and local structure, respectively. The telluric vectors are linearly polarized and rotated out off the regional coordinate system. Hence, they indicate a regional 2-D structure with strong galvanic distortion effects.

In the long-period band (Table 1c), $\delta^o = -0.6^\circ$ was found to be the optimal regional strike angle. In this coordinate system, both ellipticities again vanish, indicating the existence of a regional 2-D structure at long periods. However, the orientation of ellipse axes α^o_x and α^o_y deviate strongly from the regional coordinate system. This effect is the result of local distortion caused by the surface anomaly. According to the distortion angles $\overline{\beta}^o_x$ and $\overline{\beta}^o_y$, the sites may again be classified into two groups. Sites s01–s04, having positive $\overline{\beta}^o_y$ and negative $\overline{\beta}^o_x$, are located adjacent to the shallow conductor. In contrast, the distortion angles at stations s05–s07 located above the conductor have opposite sign. Effectively, the rotation of the regional field components adjacent to the surface conductor is less severe than above the conductor. In particular, at stations s05–s07, the regional $E^{\rm r}_x$ component (in the -0.6° rotated coordinate system) is rotated clockwise into the strike direction of the surface structure, while $E^{\rm r}_y$ is rotated counter-clockwise as a result of distortion. Thus, the surface electric field is strongly polarized in the direction of the local structure. In real measurements, such a case will result in poor correlation between the local magnetic and electric components parallel and perpendicular to the local structure, respectively, as a result of strong current channelling in the direction of the surface anomaly.

The above stated results are illustrated as a top view map in Fig. 3 for the period $T = 100$ s using stations covering the whole model area. Telluric vectors $\mathbf{e}_x$ (grey) and $\mathbf{e}_y$ (black) are plotted as ellipses (normalized by their major axes) after rotation of the impedance tensor into the regional coordinate system (which coincides in this model study with the measurement coordinate system). The position of the regional conductor is indicated by the dash-dotted lines, the solid lines mark the boundary and strike direction of the local structure. In the absence of distortion, the regional vector $\mathbf{e}^{\rm r}_x = (0, Z^{\rm r}_{yx})^T$ would be linearly polarized and oriented perpendicular to the

regional strike, i.e. to the dashed line, while $\mathbf{e}_y^{\mathrm{r}} = (Z_{xy}^{\mathrm{r}}, 0)^T$ would be parallel. Rotation of the telluric vectors is observed as a result of the presence of the surface anomaly, however they remain linearly polarized. Thus, the case of galvanic distortion is met. Outside of the surface anomaly, the E_y^{r} component ($\mathbf{e}_x^{\mathrm{r}}$) is rotated clockwise pointing towards the local conductor, while the E_x^{r} component ($\mathbf{e}_y^{\mathrm{r}}$), is slightly rotated counter-clockwise. Above the local conductor (in between the solid lines), the rotation of the regional fields is more dramatic. Because of distortion, both telluric vectors and thus both regional electric field components are rotated into the direction of the surface conductor, being almost parallel to each other.

Hence, the results given Table 1(c), where the regional strike and galvanic distortion parameters were calculated from stations s01–s07 in the period range 4–100 s, are representative for the whole model area. We may therefore conclude that the 3-D effects observed in the long-period band are consistently identified as galvanic effects from the shallow distorter and the regional coordinate system is determined with satisfying accuracy by multisite multiperiod minimization of the ellipticities of the telluric vectors.

3.2.2 3-D effects

At medium skin depths, both subsurface anomalies contribute to the observed response. The tensor is strongly 3-D and no coordinate system is found, in which both telluric vectors are linearly polarized for a range of periods. Thus, galvanic distortion models assuming a regional 2-D structure cannot adequately represent the tensor. However, using the approximations of Section 2.3.2, we can understand some of the information contained in the 3-D response.

In Figs 4(a) and (b), we have plotted the ellipticities and angles of major axes versus period for the sites s03 adjacent to and s06 above the surface conductor (compare Fig. 2, where the location of the stations is indicated) in a fixed 45° rotated frame, i.e. with the x-axis in strike direction of the local structure. Ellipse parameters of $\mathbf{e}_x$ and $\mathbf{e}_y$ are depicted in grey filled diamonds and black filled circles, respectively. The ellipticity of the telluric vector $\mathbf{e}_x$ at s03 is approximately zero for all periods ($\overline{\epsilon}_x = -0.01 \pm 0.04$), while $\overline{\epsilon}_y = 0.00 \pm 0.21$ depends on period, which is expressed in a large standard deviation. Above the conductor (site s06), $\overline{\epsilon}_y = 0.00 \pm 0.02$ vanishes, while $\overline{\epsilon}_x = 0.04 \pm 0.26$ is a function of period, respectively. Note also that, in coincidence with the corresponding ellipticity, the orientation of ellipses is either stable ($\overline{\alpha}_x = -1.0° \pm 2.4°$ at site s03 and $\overline{\alpha}_y = 0.6° \pm 1.2°$ at site s06) or a function of period ($\overline{\alpha}_y = 11.5° \pm 12.0°$ at site s03 and $\overline{\alpha}_x = -0.6° \pm 0.26°$ at site s06), respectively.

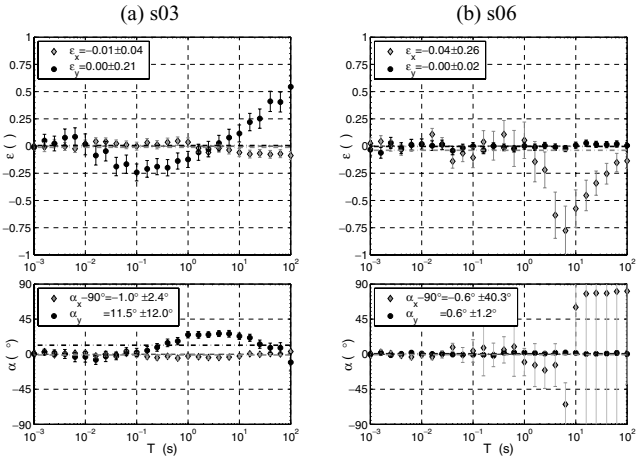

Figure 4. Example 2: ellipse parameters of telluric vectors in the local coordinate system $\delta = 45°$. Ellipticities $\epsilon_{x,y}$ and direction of major axes of ellipses $\alpha_{x,y}$ for (a) station s03 adjacent to and (b) station s06 above the local conductor. Weighted means of parameters are indicated by dash-dotted lines. One of the telluric vectors is approximately linearly polarized at all periods and indicates local B-polarization (s03) and local E-polarization (s06), respectively.

Suppose now, that the approximations of eqs (23) and (24) are valid. Then, for the present example, the polarization state of $\mathbf{e}_x$ at site s03 and $\mathbf{e}_y$ at site s06 approximately corresponds to the electric field associated with a normal magnetic field tangential and normal to the local anomaly, respectively. Here, we observe, that these telluric vectors and therefore the corresponding electric fields are predominantly linearly polarized over the whole period range, which was already anticipated previously. For an explanation, take into account that: (a) the electric field of local B-polarization adjacent to the contact dips in the (y, z) plane as a result of vertical current flow, but its projection into the horizontal plane is again dominated by the charge accumulation at the shallow lateral interface even in the presence of 3-D effects; and (b) within the surface anomaly, currents are strongly channelled, which in particular applies to those currents with the normal part in strike direction of the channel. Thus, the electric field in local B-polarization adjacent to the contact and in local E-polarization above the conductor exhibit approximately a linear polarization state, which is reflected in vanishing ellipticities of the telluric vectors in Figs 4(a) and (b), respectively.

By using the optimization scheme given in the expression of eq. (29), we may estimate for each site the coordinate system, in which one of the telluric vectors (here, $\mathbf{e}_y$) has minimal ellipticity for a range of periods. This coordinate system was referred to as local strike. Because at sites s03 and s06 the same coordinate system applies to the whole period range, we use all periods between 0.001–100 s in order to determine the local strike.

The estimated local strike directions for the model shown in Fig. 2 are plotted as top view maps in Fig. 5(a), the corresponding telluric vectors in Fig. 5(b) for the period $T = 1$ s, for which the coupling of induction effects in the shallow and the deep conductor is evident. As it can be deduced from Fig. 5(b), the ellipticities of $\mathbf{e}_y$ vanish almost exactly in the appropriate coordinate system, while $\epsilon_x \neq 0$ for most sites. This corresponds to the results for s06 (Fig. 4b), where $\epsilon_y \simeq 0$, and to s03 (Fig. 4a), but in a 180° rotated frame, because ϵ_y had been minimized. Thus, adjacent to the local conductor, the electric field in local B-polarization and, on top of the surface anomaly, the local E-polarization electric field are predominantly linearly polarized.

It is obvious from Fig. 5(a), that the local strike directions have a distinct meaning above and in the vicinity of the shallow conductor. Above the surface anomaly, they directly give the strike direction of the local anomaly, while adjacent but close to the surface anomaly, they point perpendicular to the local strike. Further away from the distorting anomaly, the strike direction is a mixture of regional and local strike or indicates the regional strike, if the influence of the local anomaly is small.

4 APPLICATION TO FIELD DATA

The previously described model study has been motivated by audiomagnetotelluric (AMT)/MT data in the period range 0.001–100 s, which we measured in Gaxun Nur Basin, an intracontinental basin structure in the Inner Mongolia province of China. This basin is of key interest for geoscientists, because its sediments are presumed to be a valuable archive for climatic and environmental signals from

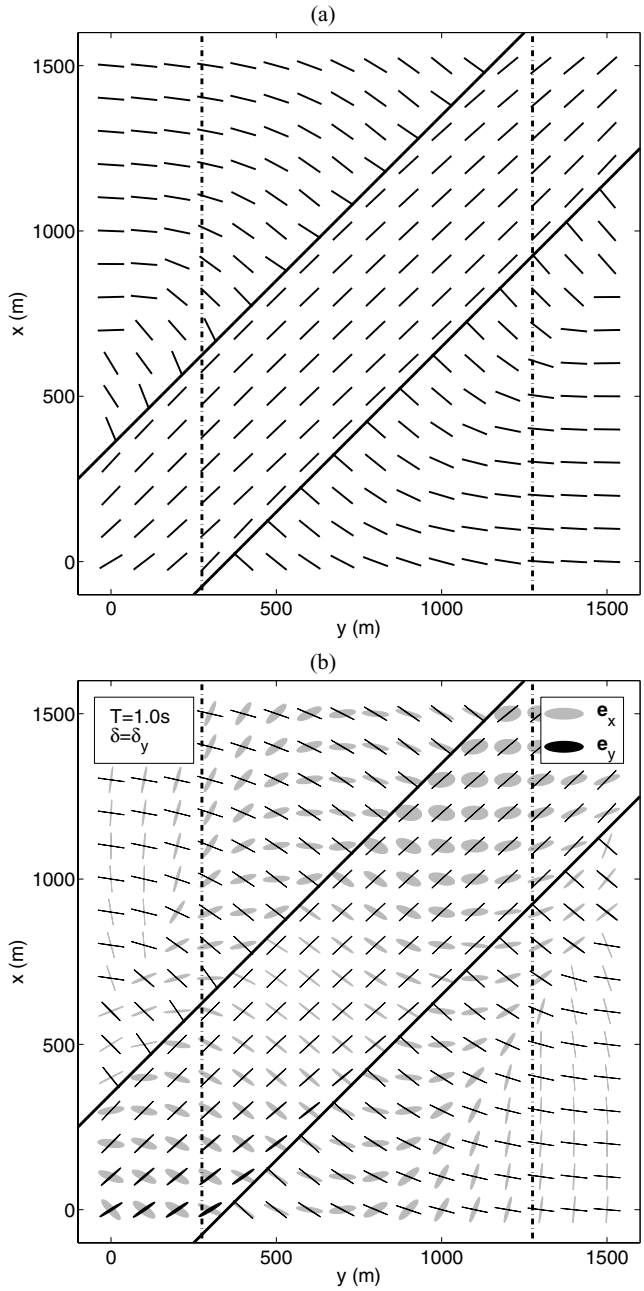

Figure 5. Example 2: local coordinate system. (a) Local strike direction obtained from minimization of only one telluric vector (here, $\mathbf{e}_y$) for the period range 0.001–100 s. Note, that the local coordinate system has an ambiguity of 180°. (b) Telluric vectors for the period $T = 1.0$ s plotted as ellipses after rotation of the impedance tensor to the directions shown in (a). The vector $\mathbf{e}_y$ is approximately linearly polarized at all points, while $\mathbf{e}_x$ has a strong ellipticity in particular above the surface conductor and in the vicinity of the crossover points of the shallow and deep conductor.

the past million years (Wuennemann & Hartmann 2002). Today, the basin is partially covered by sand dunes as a result of the hyperarid climate of the desert Gobi. Within a multidisciplinary investigation of this basin, electromagnetic measurements (transient electromagnetic, AMT/MT) were carried out across a 4-km wide northward striking wadi, a potential drainage channel in which material is discharged from the Gobi Altai mountain range into the Gaxun Nur Basin.

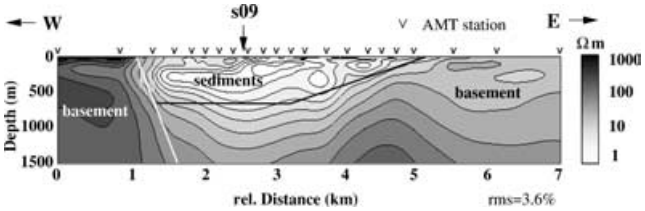

Figure 6. Field data example: 2-D joint inversion of E- and B-polarization apparent resitivities and phases for the period range (0.001–0.1 s) from 22 stations indicated by triangles at the surface. Strike direction is approximately N. The highly conducting body is suspected to act as a distorter at long periods by effectively channelling currents.

A 2-D joint inversion (Siripunvaraporn & Egbert 2000) of of E- and B-polarization apparent resistivities and phases for the upper period range of the AMT data (0.001–0.1 s) yields the resistivity model shown in Fig. 6, many features of which have also been recovered by 1-D inversion of transient electromagnetic (TEM) data. Thus, the model is well constrained. The section is divided into two different resistive crystalline rock units (black and grey) and a highly conducting body (white) corresponding to sediments in the wadi. Crystalline rocks, exposed to the east and west of the wadi, are clearly differentiable into an eastern and a western block both geologically as well as from their different resistivities. The sediments of the wadi reach a thickness of around 500 m in the western part and a width of approximately 4 km along the section. The total length of the structure is approximately 20 km, bounded to the north by metamorphic rocks and disappearing to the south under lake sediments and dunes. The low resistivity (less than 1 Ωm) of the sedimentary infill must be explained by a high concentration of dissolved salt in the pores of the sediments, which is reasonable given the background of high evaporation rates exceeding the precipitation by the order of several magnitudes.

A 500-m deep section of conducting sediments above more resistive layers is considered as a large-scale structure with respect to the shortest period of 0.001 s (skin depth ∼15 m), but it appears as a small-scale inhomogeneity for periods of 100 s (skin depth >10 km). Thus we may expect serious distortion effects for long periods, caused by the structure well resolved at short periods.

In Fig. 7, data from MT site s09, indicated in Fig. 6, are shown as an illustrating example. Rotated to the strike direction of the wadi (−12°, counter-clockwise), determined from the minimization of ellipticities of both telluric vectors within the first two period decades, apparent resistivities and phases (Fig. 7a) indicate a 1-D increase in conductivity with depth at the shortest periods. With increasing period, the sounding curves split, as the margins of the graben become included in the inductive volume.

For periods longer than ∼0.1 s, the diagonal impedance elements become increasingly important, approaching the amplitudes of the off-diagonal elements between 1–100 s. Therefore the period range for the 2-D inversion was restricted to the shortest periods.

The response characteristics are equivalently reflected in the elliptical parameters shown in Fig. 7(b): vanishing ellipticities with weighted means $\overline{\epsilon}_x = 0.00 \pm 0.00$ and $\overline{\epsilon}_y = 0.01 \pm 0.01$ of the telluric vectors $\mathbf{e}_x$ and $\mathbf{e}_y$ within the first two decades indicate 1-D or 2-D conditions, the latter in principal coordinates. Accordingly, distortion angles in this period range are constant and, moreover, vanish, indicating the absence of galvanic distortion. A sharp increase of ϵ_x at 0.1 s rising to a maximum at 1 s and slowly decaying at longer periods coincides with non-vanishing main-diagonal elements. Thus, 3-D effects are evident in the data, being either the

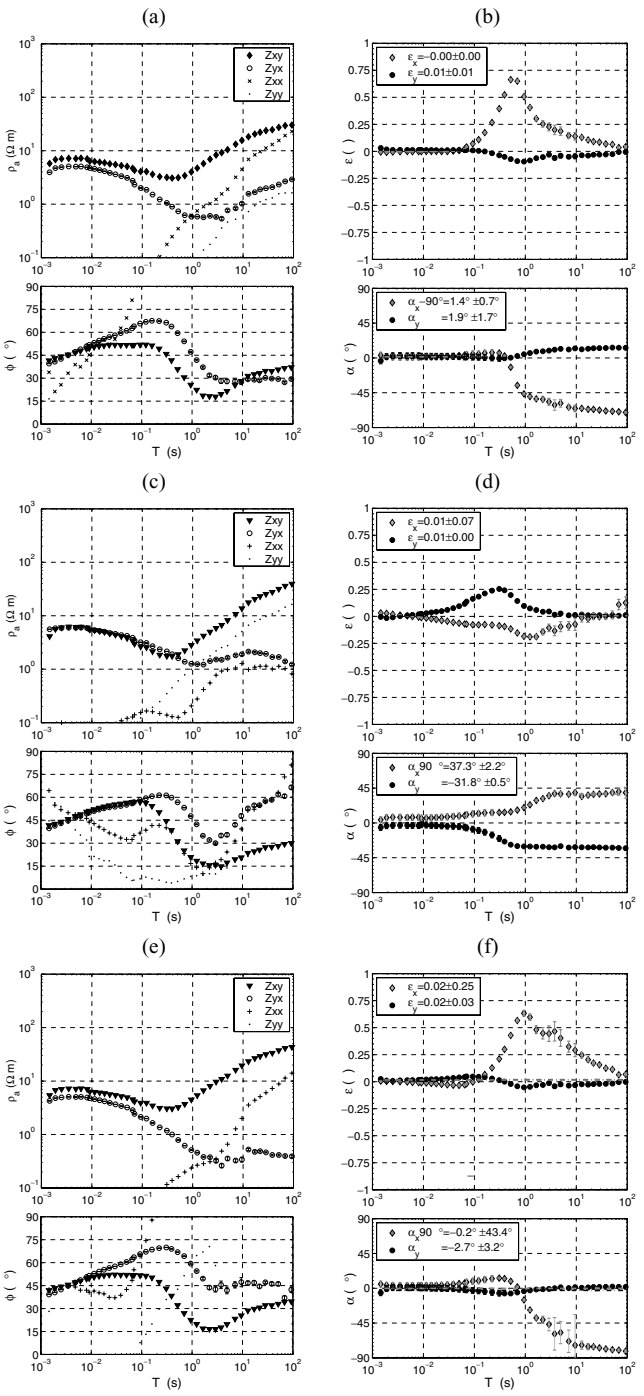

Figure 7. Field data example: site s09. (a) Apparent resistivities and phases rotated -12° (counter-clockwise) into the strike direction of the shallow conductor depicted in Fig. 6. (b) Elliptical parameters of telluric vectors in the same coordinate system. (c), (d) and (e), (f): same as (a), (b) but rotated 36.8° and 0.5° clockwise, where the first is interpreted as the regional coordinate system and the latter is the estimated local coordinate system. (See text for detailed discussion.)

result of strong 3-D structure, the distorted response of a 2-D regional structure, or a combination of both.

Application of the minimization routine (eq. 29) to the lowest decade from 10 to 100 s leads to the results shown in Figs 6(c) and (d). Vanishing ellipticities with $\overline{\epsilon}_x = 0.01 \pm 0.07$ and $\overline{\epsilon}_y = 0.01 \pm 0.00$ indicate linear polarization of the telluric vectors, which point towards a deep 2-D conductivity distribution, striking at 36.8° clockwise. Distortion angles are constant over nearly two decades from 1–100 s, approaching almost $\pm 45^\circ$. Note, that at long periods, phases of the off-diagonal elements and the corresponding main-diagonal elements are the same and related apparent resistivity curves are parallel in the double-logarithmic scale (Fig. 7c). Thus, strong distortion effects the long-period data, where the distorter has previously been postulated as the sedimentary filling of the graben shown in Fig. 6.

From these results, which are similarly observed at other stations, the following interpretation is established to explain the data:

(i) The short-period band of the sounding curve reflects the 2-D graben structure. Its strike direction is 12°W.

(ii) A deep conductor/resistor, which is also 2-D, is resolved by long periods. It is oriented 37°E, thus deviating from the surface strike by approximately 49°. This is also supported by the high distortion angles.

(iii) At intermediate periods currents are induced in both the shallow surface conductor and the deep anomaly, giving rise to strong 3-D effects.

The survey discussed above was designed for rather shallow investigations. Therefore, the distribution of stations is not suitable for a 2-D inversion of undistorted long-period data nor for a 3-D modelling in order to verify the outcome of the distortion analysis. It should also be noted, that magnetic transfer functions, which were also measured, do not strictly support the results stated above for long periods. However, the orientation of real and imaginary induction arrows in presence of 3-D structures is not well understood and often deviates from directions suggested by impedance tensor analysis.

Let us finally utilize this sounding curve to exemplarily study the 3-D characteristics of the MT impedance tensor. The measurement point is located above a conductive channel, which is (comparable to example 2) embedded in a more complicated 3-D structure. We claimed, that in such a case, there often exists a coordinate system, in which the telluric vector $\mathbf{e}_y$ vanishes approximately, if rotated to the local strike direction. The rotation angle was determined in this case to be 0.5°E by jointly minimizing ϵ_y for all periods and is close to but not exactly the strike direction used for the 2-D inversion of the short-period band. In this coordinate system, the apparent resistivities and phases are shown in Fig. 7(e), the related ellipse parameters are depicted in Fig. 7(f). Note, that $\overline{\epsilon}_y = 0.02 \pm 0.03$ approximately vanishes for the whole period range, while $\epsilon_x \neq 0$ and depends on period. Similarly, the orientation of $\mathbf{e}_y$ is stable and aligned with the local strike direction ($\overline{\alpha}_y = -2.7^\circ \pm 3.2^\circ$), while that of $\mathbf{e}_x$ changes with period. It is therefore reasonable to assume, that the polarization state of $\mathbf{e}_y$ represents that of the linearly polarized electric field in local E-polarization. The apparent resistivities in this coordinate system are composed of three elements (ρ_{xx}, ρ_{xy} and ρ_{yx}) with large amplitudes and ρ_{yy}, which has a small amplitude. This is in coincidence with our assumptions about the impedance tensor, measured above a shallow conductive anomaly.

Thus, we recover the 3-D effects inherent in the impedance tensor as a result of the presence of a local conductor also on field data.

5 CONCLUSION

We introduce an alternative parametrization of the impedance tensor in terms of elliptical parameters, which is neither underlaid by an *a priori* model assumption, as in the case of classical galvanic distortion analysis, nor is purely based on mathematical properties, as that of the SVD.

This approach can rather be considered as a combination of the SVD of the impedance tensor (LaTo; Yee & Paulson 1987) and the galvanic distortion analysis (Bahr 1988; Groom & Bailey 1989; Smith 1995). In contrast to the SVD, no orthogonal basis for the characteristic electric field vectors is imposed. Thereby, the rotation angles of the principal electric field vectors resulting from galvanic distortion may be identified. On the other hand, on minimizing dimensionless ellipticities of telluric vectors in order to identify the regional coordinate system, a natural formulation of the distortion problem has been established, which might be superior to previous formulations. Because ellipticities may only vary between zero and one and are independent of the magnitude, i.e. the absolute value of the impedances, data from different periods are directly comparable despite the intrinsic period dependency of the impedance. Thus, joint minimization of data from various periods and, moreover, stations is feasible, easily formulated and retrieves stable results.

An advantage of using eight parameters instead of seven to describe the impedance tensor is that an occasionally inappropriate *a priori* assumption is avoided. Instead, our parametrization simply states, in such a case, that the parameters are not interpretable in terms of a distortion model, but that they are still well determined. In order to validate the existence of a regional model, it is necessary to demand a strict period independency of the ellipticities and rotation angles for a range of periods. This is easily accomplished in our analysis, because we determine the strike direction and calculate the parametrization in rotated coordinates. Therefore, we also do not introduce an additional quantitative measure such as the phase-sensitive skew (Bahr 1988) to validate a regional 2-D structure (though a measure could be the root mean square weighted ellipticties). Instead, we suggest to closely inspect the range of periods in which both ellipticities vanish and in which the distortion angles are frequency independent.

In addition to the galvanic distortion analysis, the parametrization serves to explain the behaviour of a strong 3-D impedance tensor in a particular environment: in the vicinity of a surface conductor, the polarization state of one of the telluric vectors directly represents one electric field polarization, which is found to be approximately linear. Thereby, it is understood, that the impedance tensor is often composed of three large elements and one small element.

It was beyond the scope of this work to provide a detailed catalogue of 3-D model studies. It has been demonstrated, however, that the approach we suggest may serve to provide a better understanding of 3-D effects in MT impedance data and we believe that it can be helpful to adopt it to a wider class of conductivity models than the one we used.

ACKNOWLEDGMENTS

The Deutsche Forschungsgemeinschaft (DFG) has financed the measurements in China (Project Bu 298-15). Field work has been carried out together with colleagues from Lanzhou University, China. Parts of the instrumentation were supplied by the Geophysical Instrument Pool of the Geoforschungszentrum (GFZ) Potsdam. The authors thank the anonymous reviewer for his constructive comments and questions, which helped us to improve our understanding of the 3-D effects described in this paper.

REFERENCES

Bahr, K., 1988. Interpretation of the magnetotelluric impe–dance tensor: regional induction and local telluric distortion, *J. Geophys.,* **62,** 119–127.

Groom, R.W. & Bahr, K., 1992. Corrections for near surface effects: decomposition of the magnetotelluric impedance tensor and scaling corrections for regional resistivities: a tutorial., *Geophys. Surv.,* **132,** 341–379.

Groom, R.W. & Bailey, R.C., 1989. Decomposition of magnetotelluric impedance tensors in presence of local three-dimensional galvanic distortion, *J. geophys. Res.,* **94,** 1913–1925.

Groom, R.W. & Bailey, R.C., 1991. Analytic investigation of the effects of near surface 3-d galvanic scatterers on MT tensor decompositions, *Geophysics,* **56,** 496–518.

LaTorraca, G., Madden, T. & Korringa, J., 1986. An analysis of the magnetotelluric impedance tensor for three-dimensional structures, *Geophysics,* **51,** 1819–1829 (LaTo).

Mackie, R.L., Smith, J.T. & Madden, T., 1994. Three-dimensional electromagnetic modeling using finite difference equations: The magnetotelluric example, *Radio Sci.,* **29,** 923–936.

McNeice, G. & Jones, A.G., 2001. Multi-site, multi-frequency tensor decomposition of magnetotelluric data, *Geophysics,* **66,** 158–173.

Siripunvaraporn, W. & Egbert, G., 2000. An efficient data-subspace inversion for two-dimensional magnetotelluric data, *Geophysics,* **65,** 791–803.

Smith, J.T., 1995. Understanding telluric distortion matrices, *Geophys. J. Int.,* **122,** 219–226.

Weichmann, P.B., Lavely, E.M. & Ritzwoller, M.H., 2000. Theory of surface nuclear magnetic resonance with application to geophysical imaging problems, *Phys. Rev. E.,* **62,** 1290–1312.

Wuennemann, B. & Hartmann, K., 2002. Morphodynamics and paleohydrography of the Gaxun Nur Basin, Inner Mongolia, China, *Zeitschrift für Geomorphologie, Neue Folge,* **126,** 147–168.

Yee, E. & Paulson, K.V., 1987. The canonical decomposition and its relationship to other forms of magnetotelluric impedance tensor analysis, *J. Geophys.,* **61,** 173–189.

Zhang, P., Roberts, R.G. & Pedersen, L.B., 1987. Magnetotelluric strike rules, *Geophysics,* **52,** 267–278.

Zonge, K.L. & Hughes, L.J., 1991. Controlled source audiofrequency magnetotellurics, in *Electromagnetic methods in applied geophysics,* ed. Nabighian, M.N., 2nd edn, pp. 713–809, Soc. Expl. Geophys., Tulsa, OK.

APPENDIX A: REPRESENTATION OF ELLIPTICAL POLARIZATION STATES

The following ellipse parametrization has been introduced by Weichmann *et al.* (2000). It is briefly summarized in Sections A1 and A2, and the derivation of linear error propagation is given in Sections A3 and A4.

A1 Parametrization

A monochromatic vector field $\mathbf{v}$ oscillates with angular frequency ω_0 in time domain with

$$\begin{aligned}\mathbf{v}(t) &= \mathbf{A}(\omega_0)\cos(\omega_0 t) + \mathbf{B}(\omega_0)\sin(\omega_0 t)\\ &= \overline{\mathbf{A}}(\omega_0)e^{i\omega_0 t} + \overline{\mathbf{A}}^*(\omega_0)e^{-i\omega_0 t},\end{aligned} \tag{A1}$$

in which $\overline{\mathbf{A}}(\pm\omega_0) = \frac{1}{2}[\mathbf{A}(\omega_0) - i\mathbf{B}(\omega_0)] = \overline{\mathbf{A}}^*(\mp\omega_0)$ is the complex field amplitude. In general, $\mathbf{A}$ and $\mathbf{B}$ are non-collinear, corresponding to an elliptically polarized vector field.

Now, let $\mathbf{v}(t) = (v_1, v_2)^T$ and consequently $\overline{\mathbf{A}}(\omega_0)$ be a vector lying in the $z = 0$ plane and decompose it in the form

$$\overline{\mathbf{A}}(\omega_0) = e^{i\zeta(\omega_0)}\left[a(\omega_0)\widehat{\mathbf{a}}(\omega_0) + ic(\omega_0)\widehat{\mathbf{c}}(\omega_0)\right], \tag{A2}$$

where the phase ζ is chosen in such a way that a and c are real and $a \geq |c| \geq 0$. The unit vectors are given by $\widehat{\mathbf{a}} = (\cos\alpha, \sin\alpha)^T$ and $\widehat{\mathbf{c}} = \widehat{\mathbf{z}} \times \widehat{\mathbf{a}}$. Because $\overline{\mathbf{A}}(-\omega_0) = \overline{\mathbf{A}}^*(\omega_0)$, it follows that $\zeta(\omega_0) = -\zeta(-\omega_0)$ and $c(\omega_0) = -c(-\omega_0)$ are odd functions of frequency and $a(\omega_0) = a(-\omega_0)$ and $\widehat{\mathbf{a}}(\omega_0) = \widehat{\mathbf{a}}(-\omega_0)$ are even functions of frequency.

With this decomposition, we see that the total field may be written in the form

$$\mathbf{v}(t) = a\cos(\omega_0 t - \zeta)\,\widehat{\mathbf{a}} + c\sin(\omega_0 t - \zeta)\,\widehat{\mathbf{c}}. \tag{A3}$$

The first addend is denoted as the corotating part, the second as the counter-rotating part of the elliptically polarized field. The real amplitudes a and c are identified as major and minor axes of the polarization ellipse, respectively, and the phase ζ determines the vector at $t = 0$.

For notational simplicity, we rewrite eq. (A2) as

$$\mathbf{v} = e^{i\zeta}\,(a\widehat{\mathbf{a}} + ic\widehat{\mathbf{c}}), \tag{A4}$$

where now $\mathbf{v} = \mathbf{v}(\omega_0)$.

A2 Calculation of ellipse parameters

From the combinations

$$\begin{aligned}
&\mathbf{v}\cdot\mathbf{v} = (a^2 - c^2)e^{2i\zeta},\\
&\mathbf{v}\cdot\mathbf{v}^* = a^2 + c^2,\\
&\mathbf{v}\times\mathbf{v}^* = -2iac\widehat{\mathbf{z}},
\end{aligned} \tag{A5}$$

one obtains

$$e^{i\zeta} = \left[\frac{\mathbf{v}^2}{|\mathbf{v}^2|}\right]^{\frac{1}{2}} \tag{A6}$$

for the phase, and the major and minor axes are given by

$$\begin{aligned}
a &= \left[\frac{1}{2}(|\mathbf{v}|^2 + |\mathbf{v}^2|)\right]^{\frac{1}{2}},\\
c &= \operatorname{sign}(i\widehat{\mathbf{z}}\cdot\mathbf{v}\times\mathbf{v}^*)\left[\frac{1}{2}(|\mathbf{v}|^2 - |\mathbf{v}^2|)\right]^{\frac{1}{2}},
\end{aligned} \tag{A7}$$

where $a > 0$ and the sign of c may be positive or negative indicating the sense of rotation in time domain. The ellipticity is then determined from

$$\epsilon = \frac{c}{a}. \tag{A8}$$

Finally, the unit vector is

$$\widehat{\mathbf{a}} = \frac{1}{a}\Re(e^{-i\zeta}\mathbf{v}), \tag{A9}$$

from which the angle α with the x-axis can be derived:

$$\tan\alpha = \frac{1}{a}\frac{a_2\cos\zeta + b_2\sin\zeta}{a_1\cos\zeta + b_1\sin\zeta}. \tag{A10}$$

Here, we denote real and imaginary parts of v_i by a_i and b_i, respectively, i.e. $v_i = a_i + ib_i$.

A3 Variance of a, c and ϵ

Let us denote the variance of $\mathbf{v}$ by $\sigma^2_{\mathbf{v}} = (\,\sigma^2_{v_1}\quad\sigma^2_{v_2}\,)^T$, where the same standard deviation is applied to the real and imaginary part of each component. Assuming linear error propagation, then the variance of the major axis a is derived from

$$\sigma^2_a = \sum_k \left(\frac{\partial a}{\partial p_k}\right)^2 \sigma^2_{p_i}, \tag{A11}$$

where p_k denotes the variables of a, i.e. $a = a(p_k)$.

Let $v_i = a_i + ib_i$. Differentiating eq. (A7) with respect to one of the parameters $p \doteq p_k \epsilon \{a_1, b_1, a_2, b_2\}$ yields

$$\frac{\partial a}{\partial p} = \frac{1}{2a}\left(\frac{\partial|\mathbf{v}|^2}{\partial p} + \frac{\partial|\mathbf{v}^2|}{\partial p}\right), \tag{A12}$$

where

$$\frac{\partial\,|\mathbf{v}|^2}{\partial p} = 2p$$

and

$$\begin{aligned}
\frac{\partial|\mathbf{v}^2|}{\partial p} &= \frac{\pm 2p\left(a_1^2 - b_1^2 + a_2^2 - b_2^2\right)}{|\mathbf{v}^2|}\\
&\quad + \frac{4\left(1 + \frac{\partial}{\partial p}\right)(a_1b_1 + a_2b_2)}{|\mathbf{v}^2|},
\end{aligned}$$

where the negative sign is chosen, if $p \epsilon \{b_1, b_2\}$. The variance of a is summed up to

$$\begin{aligned}
\sigma^2_a &= \left[\left(\frac{\partial a}{\partial a_x}\right)^2 + \left(\frac{\partial a}{\partial b_x}\right)^2\right]\sigma^2_{v_1}\\
&\quad + \left[\left(\frac{\partial a}{\partial a_y}\right)^2 + \left(\frac{\partial a}{\partial b_y}\right)^2\right]\sigma^2_{v_2}.
\end{aligned} \tag{A13}$$

The variance of c differs from that of a only by a sign, as can easily be deduced from eq. (A7). The sign function determines only the sign of c and does not enter the squared partial derivative in the error propagation law.

Having calculated the variances of major and minor axes, the variance for the ellipticity of eq. (A8) is easily obtained by

$$\sigma^2_\epsilon = \left(\frac{\epsilon}{a}\right)^2\sigma^2_a + \left(\frac{1}{a}\right)^2\sigma^2_b. \tag{A14}$$

A4 Variances of phase ζ and directional parameter α

The radical of eq. (A6) is a complex number $|z|e^{i\phi}$, where $|z| = 1$, because $e^{i\zeta} = [|z|e^{i\phi}]^{\frac{1}{2}} = e^{i\frac{\phi}{2}}$, and $\tan\phi = \Im(\mathbf{v}^2)/\Re(\mathbf{v}^2)$, because $|\mathbf{v}^2|$ is real. Thus,

$$\tan\phi = \frac{2(a_1b_1 + a_2b_2)}{a_1^2 + b_1^2 + a_2^2 + b_2^2} \tag{A15}$$

and $2\zeta = \phi$. The partial derivative with respect to one of the variable p is given by

$$\frac{\partial\zeta}{\partial p} = \frac{1}{1 + \tan^2 2\zeta}\frac{\left(\mathbf{v}\cdot\mathbf{v}^*\frac{\partial}{\partial p} - 2p\right)(a_1b_1 + a_2b_2)}{(\mathbf{v}\cdot\mathbf{v}^*)^2}, \tag{A16}$$

which can be used to estimate the variance of ζ.

Finally, from eq. (A10)

$$\frac{\partial\alpha}{\partial p} = \frac{1}{1 + \tan^2\alpha}\frac{\partial}{\partial p}\frac{a_2\cos\zeta + b_2\sin\zeta}{a_1\cos\zeta + b_1\sin\zeta}, \tag{A17}$$

$$\frac{\partial\alpha}{\partial a} = \frac{-\tan\alpha}{1 + \tan^2\alpha}\frac{1}{a} \tag{A18}$$

and

$$\frac{\partial\alpha}{\partial\zeta} = \frac{1}{1 + \tan^2\alpha}\frac{a_1b_2 - a_2b_1}{(a_1\cos\zeta + b_1\sin\zeta)^2}, \tag{A19}$$

which yields estimates for the variance of the angle α.

APPENDIX B: MODIFIED SVD

We modify the singular vectors $\mathbf{e}_i$ and $\mathbf{h}_i$, defined from the SVD of an impedance tensor $\mathbf{Z}$ as

$$\mathbf{Z} = \begin{bmatrix} \mathbf{e}_1 & \mathbf{e}_2 \end{bmatrix} \mathbf{Z}^{\mathrm{r}} \begin{bmatrix} \mathbf{h}_1 & \mathbf{h}_2 \end{bmatrix}, \tag{B1}$$

using eq. (A4) as

$$\mathbf{e}_i' = \mathbf{e}_i e^{-i\zeta_{e,i}} = (a_{e,i}\widehat{\mathbf{a}}_{e,i} + ic_{e,i}\widehat{\mathbf{c}}_{e,i}) \tag{B2}$$

and

$$\mathbf{h}_i' = \mathbf{h}_i e^{-i\zeta_{h,i}} = (a_{h,i}\widehat{\mathbf{a}}_{h,i} + ic_{h,i}\widehat{\mathbf{c}}_{h,i}). \tag{B3}$$

The modified SVD parametrization as suggested in LaTo reads as

$$\mathbf{Z} = \mathbf{U}_e \mathbf{M} \widetilde{\mathbf{U}}_h, \tag{B4}$$

where the phase modified singular vectors $\mathbf{e}_i'$ and $\mathbf{h}_i'$ are used as the columns of the matrices $\mathbf{U}_e$ and $\mathbf{U}_h$, respectively, instead of the singular vectors themselves. Expanding eq. (B4) yields directly for the elements of $\mathbf{M} = \mathrm{diag}(\mu_1, \mu_2)$

$$\mu_i = r_i e^{i(\zeta_{e,i} - \zeta_{h,i})}. \tag{B5}$$

Thus, the appropriate phase factors as defined in appendix B of LaTo are identified as the initial phases of the ellipse representation of eq. (A4).

APPENDIX C: SVD OF A GALVANICALLY DISTORTED 2-D IMPEDANCE TENSOR

In this section, we repeatedly take reference to formulae from LaTo.

The calculations are, for simplicity, performed in the regional coordinate system. The results, however, apply to any coordinate system.

As observed by Groom & Bailey (1991), the result of the modified SVD for a galvanically distorted impedance tensor of the form of eq. (3) with $g_x = g_y = 1$,

$$\mathbf{Z} = \mathbf{D}\mathbf{Z}^{\mathrm{r}} = \mathbf{U}_e \mathbf{M} \widetilde{\mathbf{U}}_h = \begin{bmatrix} -\sin\beta_y Z^{\mathrm{r}}_{yx} & \cos\beta_x Z^{\mathrm{r}}_{xy} \\ \cos\beta_y Z^{\mathrm{r}}_{yx} & \sin\beta_x Z^{\mathrm{r}}_{xy}, \end{bmatrix} \tag{C1}$$

has the following properties.

(i) The ellipticities ϵ_e of the modified left-singular vectors $\mathbf{e}_i$ vanish exactly.

(ii) The ellipticities ϵ_h of the modified right-singular vectors $\mathbf{h}_i'$ vanish, if the phases of the regional impedance elements are equal (or if their difference is equal π).

(iii) The orientations of modified singular vectors do not coincide with any of the directions given by the distortion angles nor the regional coordinate system.

Additionally, if $\beta_x = \beta_y \doteq \beta$, we found the following.

(iv) β is the angle, the $\mathbf{e}_i'$ are rotated out of the regional coordinate system.

(v) ϵ_h vanishes exactly.

(vi) $\mathbf{h}_i'$ are linearly polarized and span the regional coordinate system.

These statements are easily proven using the formulae in LaTo (their eqs 26, 27, 32 and 33). Consider first the hermitian matrix $\mathbf{C}_{e,h}$ defined as

$$\mathbf{C}_h = \mathbf{Z}\widetilde{\mathbf{Z}} \tag{C2}$$

(eq. 26 of LaTo) and

$$\mathbf{C}_e = \mathbf{Z}\widetilde{\mathbf{Z}} \tag{C3}$$

(eq. 27 of LaTo), which are expanded to

$$\begin{aligned} C_{h,xx} &= \left|Z^{\mathrm{r}}_{yx}\right|^2 \sin^2\beta_y + \left|Z^{\mathrm{r}}_{xy}\right|^2 \cos^2\beta_y, \\ C_{h,xy} &= \cos\beta_y \sin\beta_x Z^{\mathrm{r}}_{xy} Z^{r*}_{yx} - \cos\beta_x \sin\beta_y Z^{\mathrm{r}}_{xy} Z^{r*}_{yx}, \\ C_{h,yx} &= \cos\beta_y \sin\beta_x Z^{r*}_{xy} Z^{\mathrm{r}}_{yx} - \cos\beta_x \sin\beta_y Z^{r*}_{xy} Z^{\mathrm{r}}_{yx}, \\ C_{h,yy} &= \left|Z^{\mathrm{r}}_{yx}\right|^2 \cos^2\beta_y + \left|Z^{\mathrm{r}}_{xy}\right|^2 \sin^2\beta_y \end{aligned} \tag{C4}$$

and

$$\begin{aligned} C_{e,xx} &= \left|Z^{\mathrm{r}}_{yx}\right|^2 \sin^2\beta_y + \left|Z^{\mathrm{r}}_{xy}\right|^2 \cos^2\beta_x, \\ C_{e,xy} &= \left|Z^{\mathrm{r}}_{xy}\right|^2 \sin\beta_x \cos\beta_x - \left|Z^{\mathrm{r}}_{yx}\right|^2 \sin\beta_y \cos\beta_y, \\ C_{e,yx} &= \left|Z^{\mathrm{r}}_{xy}\right|^2 \sin\beta_x \cos\beta_x - \left|Z^{\mathrm{r}}_{yx}\right|^2 \sin\beta_y \cos\beta_y, \\ C_{e,yy} &= \left|Z^{\mathrm{r}}_{yx}\right|^2 \cos^2\beta_y + \left|Z^{\mathrm{r}}_{xy}\right|^2 \sin^2\beta_x, \end{aligned} \tag{C5}$$

respectively.

The ellipticities $\epsilon_e = \tan\nu_e$ of the modified electric singular vectors are derived from eq. (33) of LaTo,

$$\sin 2\nu_e = \frac{i\left(C_{e,xy} - C_{e,yx}\right)}{r_1^2 - r_2^2}, \tag{C6}$$

where r_i are the singular values of $\mathbf{Z}$. Because $C_{e,\mathrm{xy}} = C_{e,yx}$ as seen from eq. (C5), the nominator in eq. (C6) vanishes and thus $\nu_e = 0$ and $\epsilon_e = 0$ independent of the singular values. Thus, the left-singular vectors are linearly polarized.

Denote now the angle γ_e as the angle of the major axes of $\mathbf{e}_1$ with the x-axis. It is calculated with eq. (32) of LaTo as

$$\tan 2\gamma_e = \frac{C_{e,xy} + C_{e,yx}}{C_{e,xx} - C_{e,yy}}. \tag{C7}$$

Expanding as before leads to a mixture of the absolute values of the regional impedances and sines and cosines of the distortion angles, respectively. If, however, $\beta_x = \beta_y = \beta$, eq. (C7) simplifies to $\tan 2\gamma_e = \tan 2\beta$, thus

$$\gamma_e = \beta, \tag{C8}$$

i.e. the direction of the left-singular vectors is determined by the distortion angle β.

Eq. (C4) shows that $C_{h,\mathrm{xy}} = C^*_{h,yx}$. If $\arg(Z_{\mathrm{xy}}) + \pi = \arg(Z_{yx})$, i.e. the regional impedances have the same phase, then $C_{h,\mathrm{xy}} = C^*_{h,\mathrm{xy}}$ becomes real. Thus, applying formula in eq. (C6) to the right-singular vectors $\mathbf{h}_i$, its nominator vanishes. Therefore, the ellipticity

$$\epsilon_h = \tan 2\nu_h \tag{C9}$$

vanishes, if the impedance elements have the same phase. If $\beta_x = \beta_y = \beta$ again, $C_{h,\mathrm{xy}} = C_{h,yx} = 0$ independent of the impedance phases and thus $\epsilon_h = 0$ as well.

Only in the latter case it can be shown using eq. (C7) that

$$\gamma_h = 0, \tag{C10}$$

i.e. the direction of right-singular vectors coincides with the regional frame. Otherwise, the direction of $\mathbf{h}_i$ is an algebraic mixture of the regional impedances and the distortion angles.

These results state that the SVD indicates the existence of a regional 2-D structure, if the left-singular vectors are linearly polarized. If the right-singular vectors are also linearly polarized, and the phases of the regional impedances are not equal, then the right-singular vectors indicate the regional coordinate system. This is however only the case, if $\beta_x = \beta_y$. Then, the deviation of the left-singular vectors from the regional frame yields the distortion angle. The equality of regional phases may be deduced from equal phases of the characteristic values μ_i.

In a rotated coordinate system, e.g. $\mathbf{Z} = \mathbf{RDZ}^{\mathrm{r}}\,\mathbf{R}^T$, the SVD yields the same polarization states, but the directions of singular vectors are altered. In analogy to the previous results, it is now a straightforward calculation to show for the case $\beta_x = \beta_y = \beta$ that

$$\begin{aligned}
\mathbf{R} &= \mathbf{U}_h \begin{bmatrix} 0 & 1 \\ 1 & 0 \end{bmatrix}, \\
\mathbf{D} &= \begin{bmatrix} 0 & 1 \\ 1 & 0 \end{bmatrix} \mathbf{U}_h^T \mathbf{U}_e, \\
\mathbf{Z}^{\mathrm{r}} &= \begin{bmatrix} -1 & 0 \\ 0 & 1 \end{bmatrix} \mathbf{M} \begin{bmatrix} 0 & 1 \\ 1 & 0 \end{bmatrix},
\end{aligned} \tag{C11}$$

where $\mathbf{U}_h$ and $\mathbf{U}_e$ are real. More precisely, $\mathbf{U}_h$ is the mirrored rotation matrix and $\mathbf{U}_e$ is a function of the distortion angle β, i.e. performs an additional rotation of the regional electric field components out of the regional coordinate system.